Biosensors and Bioelectronics 73 (2015) 174–180

Contents lists available at ScienceDirect

Biosensors and Bioelectronics

journal homepage: www.elsevier.com/locate/bios

Dual aptamer-immobilized surfaces for improved affinity through multiple target binding in potentiometric thrombin biosensing

Tatsuro Goda [a,*], Daiki Higashi [a,b], Akira Matsumoto [a], Toru Hoshi [b], Takashi Sawaguchi [b], Yuji Miyahara [a,*]

[a] Institute of Biomaterials and Bioengineering, Tokyo Medical and Dental University (TMDU), 2-3-10 Kanda-Surugadai, Chiyoda, Tokyo 101-0062, Japan
[b] Department of Materials and Applied Chemistry, College of Science and Technology, Nihon University, 1-8-14 Kanda-Surugadai, Chiyoda, Tokyo 101-8308, Japan

ARTICLE INFO

Article history:
Received 22 April 2015
Received in revised form
25 May 2015
Accepted 29 May 2015
Available online 2 June 2015

Keywords:
DNA aptamer
Thrombin
Field-effect transistors
Self-assembled monolayers
Cyclic voltammetry
Chronocoulometry

ABSTRACT

We developed a label-free and reagent-less potentiometric biosensor with improved affinity for thrombin. Two different oligomeric DNA aptamers that can recognize different epitopes in thrombin were introduced in parallel or serial manners on the sensing surface to capture the target via multiple contacts as found in many biological systems. The spacer and linker in the aptamer probes were optimized for exerting the best performance in molecular recognition. To gain the specificity of the sensor to the target, an antifouling molecule, sulfobeaine-3-undecanethiol (SB), was introduced on the sensor to form a self-assembled monolayer (SAM). Surface characterization revealed that the aptamer probe density was comparable to the distance of the two epitopes in thrombin, while the backfilling SB SAM was tightly aligned on the surface to resist nonspecific adsorption. The apparent binding parameters were obtained by thrombin sensing in potentiometry using the 1:1 Langmuir adsorption model, showing the improved dissociation constants (K_d) with the limit of detection of 5.5 nM on the dual aptamer-immobilized surfaces compared with single aptamer-immobilized ones. A fine control of spacer and linker length in the aptamer ligand was essential to realize the multivalent binding of thrombin on the sensor surface. The findings reported herein are effective for improving the sensitivity of potentiometric biosensor in an affordable way towards detection of tiny amount of biomolecules.

1. Introduction

Label-free electrical biosensing using a field-effect transistor (FET) and ion-sensitive FET (ISFET) is a powerful technique for detecting biomolecules and biochemical reactions in amperometric, potentiometric, and capacitive formats (Bergveld, 2003; Goda et al., 2015; Lee et al., 2009; Matsumoto et al., 2009; Palazzo et al., 2015; Poghossian et al., 2005; Schoning and Poghossian, 2006). The fabrication of FET biosensor is compatible to the complementary metal oxide semiconductor (CMOS) process (Graham et al., 2011) so that it is straightforward to downsizing, high integration, and low-cost production for providing a new modality for home healthcare and decentralized diagnosis by realizing miniaturized and easy-to-operate type of devices. A key issue for measuring biomolecules underlies the development of functional bio-interface which shows a high affinity and selectivity to an analyte on the gate surface in contact with a biological sample. So far, a range of ligands and receptors from natural and synthetic origins has been employed on the gate electrode to show an affinity to a target molecule. The recognition event should occur within the electrical double layer at the electrode–solution interface since the transducing mechanism is based on the field effect, namely the electrostatic interaction of carriers in the semiconductor (i.e., electrons or holes) with innate charges of biomolecule as an analyte. Charges of target molecule located outside the double layer are screened by mobile counterions in an electrolyte solution. The characteristic screening length (i.e., the solution Debye length) results in less than one nanometers under physiological ionic strengths, meaning that an antibody as a general ligand in immunoassays for proteins may not be used in a physiologically relevant ionic strength for the charge detection system due to its relatively large size of tens nanometers (Bukar et al., 2014; Stern et al., 2007b). Therefore, most of the field effect-based immunosensors are operated at low salt concentrations of typically less than 1 mM (Elfstrom et al., 2008; Im et al., 2007; Kim et al., 2010; Lin et al., 2010; Stern et al., 2007a, 2010; Tang et al., 2009; Zheng et al., 2005). A fragmented antibody may be

* Corresponding authors.
E-mail addresses: goda.bsr@tmd.ac.jp (T. Goda), miyahara.bsr@tmd.ac.jp (Y. Miyahara).

http://dx.doi.org/10.1016/j.bios.2015.05.067
0956-5663/

alternatively used as a small capturing element (Elnathan et al., 2012; Kim et al., 2008b), but they generally impose reduced binding affinity and selectivity.

Aptamer is a new class of molecular recognition element composed of a selected short sequence of peptides or nucleic acids by screening through the process called systematic evolution of ligands by exponential enrichment (SELEX) (Darmostuk et al., in press; Stoltenburg et al., 2007). The engineered aptamer is an alternative to antibody with advanced features on chemical and thermal stability, equal quality, and ease of structural design and chemical modification (Famulok and Mayer, 2011; Li et al., 2010; Palchetti and Mascini, 2012; Zhou et al., 2010). Importantly, its small size of a few nanometers comparable to the thickness of electrical double layer allows the target recognition event close to the gate surface without shielding the charges by mobile counterions (Goda and Miyahara, 2012a, 2013; Lee et al., 2008). Recent developments have realized the discovery of many aptamers showing the excellent affinity in terms of the dissociation constant (K_d) at subnanomolar or nanomolar levels for various target species (Jayasena, 1999; Taylor et al., 2014). Nevertheless, the binding ability is generally superior in antibody to aptamer.

In parallel to the continuous challenges in exploring better aptamers, an effort should be made for developing known aptamer-based interface with improved affinity to allow ultrasensitive biosensing towards early cancer diagnosis and single molecule detection. In biological systems, multivalent interactions are involved for producing a high affinity in molecular recognition (Mammen et al., 1998). Learning from nature, we designed biointerfaces to capture protein via cooperative interactions using existing anti-protein aptamers targeting different epitopes. The use of different aptamer sequences for targeting different binding sites in single analyte is feasible since the SELEX process can pick up several candidate sequences at a time (Darmostuk et al., in press; Stoltenburg et al., 2007). In a model study, we demonstrated the concept through the interaction between thrombin and antithrombin aptamers. Thrombin is a serine protease pro-coagulant factor by converting soluble fibrinogen to insoluble fibrin that agglutinates platelets at the site of tissue injury. Thrombin is recognized as a biomarker for several diseases because thrombin is a critical mediator of coagulation, inflammation, and angiogenesis, leading to the development of atherosclerosis, progression of cancer, and growth of tumor (Borissoff et al., 2009; Nierodzik and Karpatkin, 2006). Due to the importance of clinical diagnostics of thrombin, researchers have employed many sensing techniques including electrochemistry (Wang et al., 2009), impedance spectroscopy (Loo et al., 2012), electrochemiluminescence (Jie and Yuan, 2012), colorimetry (Liang et al., 2011), fluorescent spectroscopy (Kong et al., 2013), surface plasmon resonance (Jalit et al., 2013), and so on. Here, we performed a fine control of molecular structure of the aptamers to investigate the factors that may facilitate the multivalent binding such as immobilization format and spacer/linker lengths. Possibility and limitation are discussed in developing a dual aptamer-based nanointerface for improved affinity through bivalent attachments in the FET-based potentiometric biosensing.

2. Materials and method

2.1. Materials

Thrombin from human plasma was obtained from Calbiochem (Merck Millipore, Billerica, MA, USA). Thrombin-binding DNA aptamers with 5′-SH-$(CH_2)_6$-functionalization were purchased from Tukuba Oligo Services (Tsukuba, Ibaraki, Japan). Sulfobetaine-3-undecanethiol (SB) was obtained from Dojindo (Mashiki, Kumamoto, Japan). All the other reagents with extra pure grades were from commercial sources and were used without further purifications. Screen-printed 10-channel gold microelectrode with 500 μm in diameter was formed on a glass-epoxy resin chip and the remaining wiring circuit on the chip was insulated by coating with a SU-8 photoresist.

2.2. Self-assembled monolayer (SAM) formation

The thiol-modified DNA aptamers (2 or 10 μM in final concentration) were immobilized on a 10-channel gold microelectrode array in a reaction buffer (10 mM Tris(hydroxymethyl)aminomethane–hydrochloride (Tris–HCl), 100 mM KCl, 100 mM NaCl, 10 mM $CaCl_2$, 10 mM $MgCl_2$, and 1 mM Tris(2-carboxyethyl)phosphine hydrochloride (TCEP)) for overnight, followed by rinse with water. The remaining gold surface was backfilled by immersing in 1 mM SB aqueous solution containing 1 mM TCEP, followed by rinse with water. The modified electrodes were kept dry in dark at 4 °C until use. The SAM film on the electrode was stable during the measurement for several hours or under the storage in a deoxidized environment for at least one week.

2.3. Electrochemical measurements

Cyclic voltammetry (CV) and chronocoulometry (CC) were performed using an Autolab PGSTAT302 Potentiostat (Metrohm, Herisau, Switzerland). A planar gold thin-film modified with SAM as a working electrode, a platinum wire ($\varphi = 1$ mm) as a counter electrode, a silver/silver chloride wire as a reference electrode in 3.3 M KCl solution with a salt bridge were used. CV scans were performed from −0.1 to −1.3 V at the scan rate of 0.5 V/s in degassed 0.5 M potassium hydroxide solution. CC was conducted in 1 mM Tris–HCl buffer (pH 8.0) with and without 50 μM hexamine ruthenium(III) chloride (RuHex) under the double potential step from 0 V to −0.5 V (for one second) to 0 V.

2.4. Potentiometry

The potentiometric response of the SAM-functionalized gold electrode as a function of varying thrombin concentration was determined using a high-input impedance electrometer (Keythley 6517B, Cleveland, OH, USA) at no DC bias voltage versus the Ag/AgCl (in 3.3 M KCl solution with a salt bridge) reference electrode. Electrolyte composition of measurement buffer (pH 8.2) was 10 mM Tris–HCl, 5 mM KCl, 3 mM NaCl, 1 mM $CaCl_2$ and 1 mM $MgCl_2$. For measurements at pH 6.0, 10 mM 2-(N-morpholino) ethanesulfonic acid (MES) was used instead of 10 mM Tris–HCl. Aptamers immobilized on the electrode were denatured at 100 °C in the measurement buffers and then were annealed by cooling down to 25 °C, followed by incubation for overnight. The potential of 10-channel working electrodes were stabilized for initial 150 min in the measurement buffer, thereafter the potentials were recorded by increasing thrombin concentrations (0–1300 nM) for each 10 min at 25 °C. Data were represented as mean ± standard deviation (SD) from three sets of the 10-channel microelectrode measurements. The limit of detection (LOD) was based on 3 SD. Sensor stability was evaluated by relative standard deviation (RSD) in percent from a dataset of the 10-channel microelectrode measurements.

2.5. Apparent binding constant

Binding parameters such as the apparent binding constant (K_d) of thrombin onto the SAM-modified surface were determined by fitting the potentiometric signals as a function of thrombin concentration using 1:1 Langmuir adsorption model. Reproducibility

of the binding constants from each dataset of 10-channel microelectrode measurements was evaluated by %RSD of three independent assays.

3. Results and discussion

3.1. Preparation and characterization of multicomponent SAMs

We designed bio-interface with two different known aptamer sequences for thrombin recognition via multiple binding; the first is the "Bock" aptamer 5′-GGT TGG TGT GGT TGG-3′ which interacts with fibrinogen-binding site, and the second is the "Tasset" aptamer 5′-AGT CCG TGG TAG GGC AGG TTG GGG TGA CT-3′ which recognizes heparin-binding site (Fig. 1) (Bock et al., 1992; Tasset et al., 1997). The 5′-end of these aptamers was functionalized with hexanethiol moiety with repeating thymine sequences (5′-SH-$(CH_2)_6$-T_m-, $m=3$, 6, or 9) as a functional spacer to allow covalent contact onto a gold substrate with an increased freedom of mobility for surface-immobilized aptamers. Moreover, we designed the aptamers with a serial connection of Bock and Tasset sequences via repeating thymine sequences as an intramolecular linker (5′-SH-$(CH_2)_6$-T_m-[Boc]-T_n-[Tas]-3′, $n=0$, 5, or 10) to render multiple binding sites for thrombin on a single aptamer chain. Since the epitopes for Bock and Tasset aptamers are 3.4 nm apart in the thrombin molecule (Hasegawa et al., 2008), we optimized the spacer and linker lengths for achieving the bivalent contacts between the ligands and thrombin. The grafting of the macromolecular aptamers onto the substrate cannot fully cover the surface due to the excluded volume effect by the aptamer chains themselves. Therefore, the remaining surface was backfilled with SB for making the mixed SAM in the second step, whose zwitterionic sulfobetaine end-group dramatically reduces nonspecific adsorption of biomolecules (Holmlin et al., 2001; Smith et al., 2012). Preparation of an anti-fouling surface is critical for label-free technologies to obtain a specific signal. The introduction of SAM also helps to decrease the electrical capacitance at the interface (C_{int}), thereby increasing the potentiometric signal (ΔV) from a direct readout of net-charges of captured biomolecules

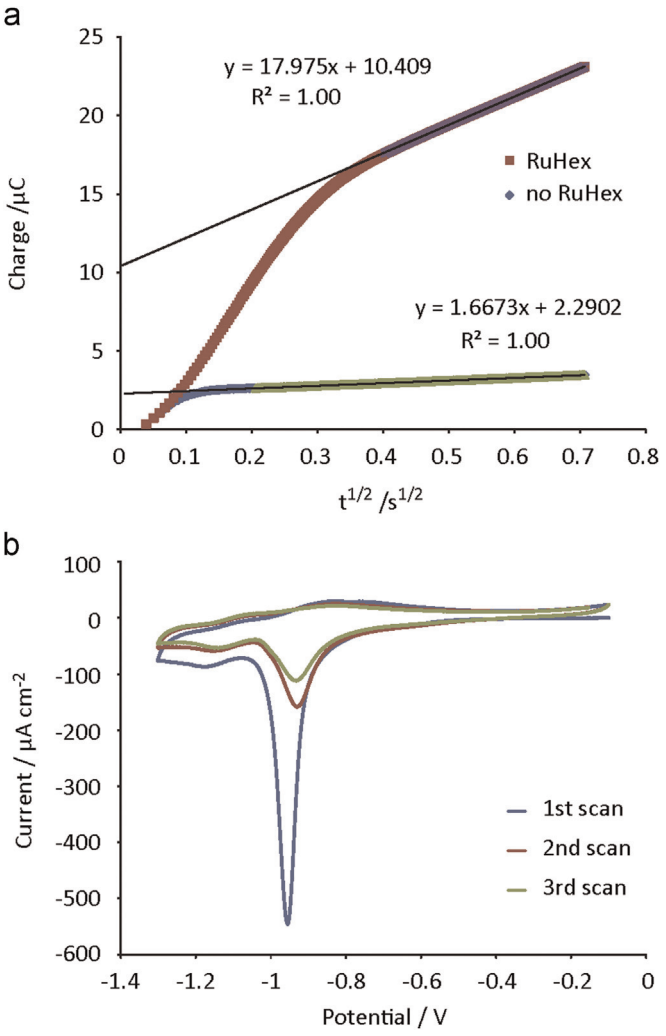

Fig. 2. Surface characterization by electrochemical methods. (a) A representative chronocoulometric curves for T_9-Boc/T_9-Tas surface with and without RuHex. (b) Cyclic voltammograms for T_9-Boc/T_9-Tas surface.

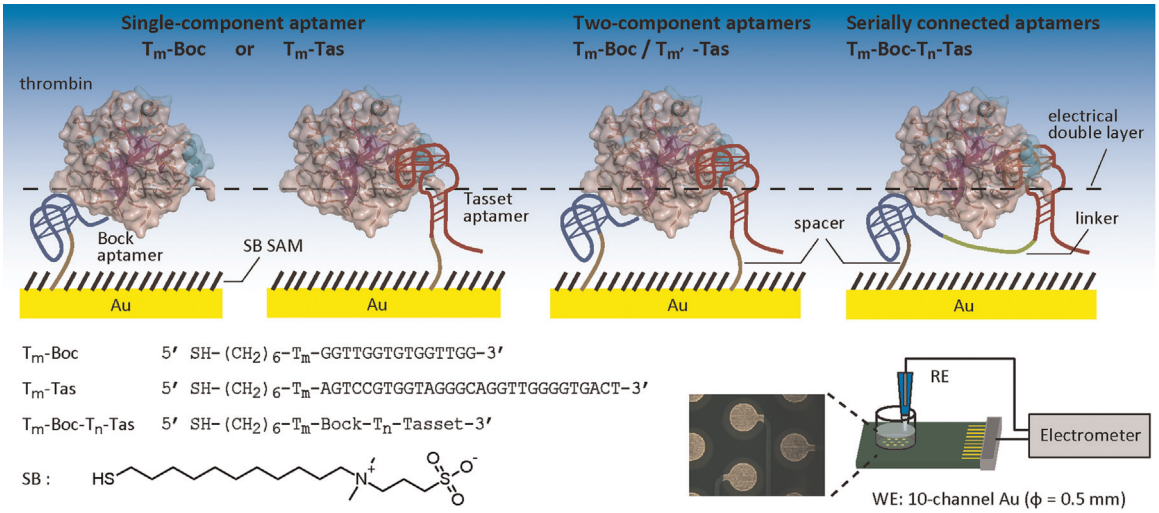

Fig. 1. A schematic illustration of electrical thrombin sensing using dual aptamer surfaces for improving the affinity by introducing multiple binding contacts between the aptamers and thrombin under optimal spacer and linker lengths at the nanointerface. Oligo DNA aptamers are small whose dimensions are comparable to the thickness of electrical double layer to perform direct electrical readout of net-charges of thrombin in potentiometry. The label-free technique requires a specific target recognition by suppressing nonspecific adsorption through the antifouling SB SAM. WE: working electrode, RE: reference electrode.

(ΔQ) based on the following equation; (Goda and Miyahara, 2013).

$$\Delta V = \Delta Q / C_{int} \quad (1)$$

For sample nomenclature, we used "T_m-Boc/$T_{m'}$-Tas" and "T_m-Boc-T_n-Tas" for the SB SAM surfaces modified with two-component aptamers and the serially connected aptamer with different spacer and linker lengths, respectively. For control experiments, we prepared single aptamer surfaces referred as "T_m-Boc" and "T_m-Tas".

The surface density of the immobilized DNA aptamers (Γ_{DNA}) in the mixed SAM was determined by chronocoulometry (CC) using a cationic redox marker RuHex (Fig. 2a) (Steel et al., 1998). The detection principle is based on the difference in the redox signal appeared as a y-intercept value in the semilogarithmic chronocoulometric graph under the conditions with and without RuHex (ΔQ_{CC}). Because the number of adsorbed RuHex molecules is electrostatically stoichiometric (1:3) to that of the DNA unit (m) in the aptamer at the electrode–solution interface as shown in the following equation;

$$\Gamma_{DNA} = (\Delta Q_{CC} N_A / FA)(3/m) \quad (2)$$

where F, A, and N_A represent Faraday's constant, geometric electrode surface area, and Avogadro's number, respectively. An overall average Γ_{DNA} was 0.041 ± 0.016 and 0.040 ± 0.016 chain/nm^2 at 10 μM and 2 μM DNA aptamers in the immobilization solutions respectively (Tables 1 and S1). Thus, an average lateral distance of aptamer chain was calculated to be 5.3 ± 1.2 nm. The concentration-independent surface density indicates the limit of congestion for macromolecular DNA aptamers (M_w=5.6–18 kDa) by the excluded volume effect under the situation of molecular crowding on a planar surface. This effect is explained by a scaling law of the radius of gyration (R_g) for graft aptamer in a good solvent as (Smith et al., 1996);

$$R_g \sim M_w^{\,n} \quad (3)$$

In fact, the average lateral distance was proportional to the number of DNA bases (Fig. S1). As a result of the effect, as well as the electrostatic repulsion between the anionic aptamers, the average distance of ligand in dual aptamer surface was longer than that of binding epitopes (3.4 nm) in the thrombin by 1.9 nm (Hasegawa et al., 2008).

The SAM density was determined from the reduction peak area (Q_{SAM}) of gold–thiol bond at −0.95 V versus the Ag/AgCl reference electrode at the first scan in cyclic voltammetry (CV) (Fig. 2b) using the following equation (Yang et al., 1996):

$$\Gamma_{SAM} = Q_{SAM} N_A / FA \quad (4)$$

The SAM density for each condition is summarized in Table S1. An average SAM density among the conditions investigated was 4.9 ± 0.4 chains/nm^2, in agreement with a theoretically maximum surface coverage of thiol compounds on Au(111) surface (Fig. S2) (Poirier and Tarlov, 1994). Therefore, an average molecular distance in SAM was 4.5 ± 0.2 Å so that the degree of SAM crowding was high by comparing the size of thrombin ($8.8 \times 6.8 \times 6.1$ nm^3) (Bode et al., 1989). Dramatic decreases in the reduction peak in the second and third scans of CV indicate an irreversible detachment of the tightly packed SB SAM under the CV measurement condition.

3.2. Potentiometric thrombin sensing using dual aptamer surfaces

We measured cumulative dose-response curves for the binding of thrombin onto the SAM containing dual aptamers using real-time label-free potentiometry (Fig. 3). The aptamers-modified working electrode was connected to the gate of FET in an electrometer (Fig. 1). Potentiometry detects local net-charges of the captured protein in the small sensing depth (the solution Debye length; κ^{-1}) compared with the size of protein due to the charge screening effect by counterions. The solution Debye length was calculated to be about 2.1 nm in the measurement buffers as follows;

$$\kappa^{-1} = \left(\varepsilon_r \varepsilon_0 k_B T / 2 n_i z^2 e^2\right)^{1/2}$$

where ε_r, ε_0, k_BT, n_i, z, and e represent the relative dielectric constant, the vacuum permittivity, the Boltzmann energy, ion concentration, ion valence, and elementary charge, respectively. The length was almost equivalent to the dimension of Bock aptamer (~2.2 nm) as determined from protein data bank (PDB, 1HAO) using PyMOL software (Fig. S3), suggesting a direct electrical readout of thrombin charges on recognition. Potential change depends on orientation and conformation of protein on the electrode surface because intrinsic charges of protein are heterogeneously distributed on the surface (Goda et al., 2012; Goda and

Table 1
A summary of aptamer probe distance (at 2 μM), binding constants (K_d and ΔV_{max}), and the limit of detection (LOD) for potentiometric thrombin sensing using the aptamer-modified SB SAM surfaces at pH 8.2 and pH 6.0. The top three values are highlighted in bold.

Entry	Aptamer distance, nm	pH 8.2 K_d, nM	ΔV_{max}, mV	LOD, nM	pH 6.0 K_d, nM	ΔV_{max}, mV	LOD, nM
T_3-Boc/T_3-Tas	5.1	670 ± 400	6.9 ± 1.5	83	84 ± 10	**41 ± 10**	17
T_3-Boc/T_6-Tas	4.9	500 ± 150	5.5 ± 3.7	80	60 ± 34	18 ± 14	**5.5**
T_3-Boc/T_9-Tas	5.8	510 ± 280	7.8 ± 0.7	33	**41 ± 32**	11 ± 7.3	8.6
T_6-Boc/T_3-Tas	4.7	460 ± 220	5.5 ± 4.4	71	62 ± 34	19 ± 13	15
T_6-Boc/T_6-Tas	**3.9**	670 ± 460	6.1 ± 1.4	87	**47 ± 20**	19 ± 13	**6.3**
T_6-Boc/T_9-Tas	6.1	650 ± 250	8.2 ± 2.9	71	60 ± 11	21 ± 12	14
T_9-Boc/T_3-Tas	5.3	610 ± 260	8.8 ± 2.5	43	56 ± 3.3	16 ± 5.1	14
T_9-Boc/T_6-Tas	5.2	**400 ± 190**	6.4 ± 0.9	45	67 ± 4.4	18 ± 4.2	15
T_9-Boc/T_9-Tas	5.1	**370 ± 71**	8.6 ± 1.1	36	63 ± 23	20 ± 8.0	9.8
T_3-Boc-T_0-Tas	6.5	500 ± 110	5.3 ± 2.9	46	68 ± 13	**36 ± 1.0**	21
T_3-Boc-T_5-Tas	7.9	**390 ± 290**	7.2 ± 6.7	68	63 ± 25	26 ± 8.2	20
T_3-Boc-T_{10}-Tas	8.3	510 ± 84	**9.5 ± 0.9**	39	**54 ± 4.7**	18 ± 12	20
T_6-Boc-T_5-Tas	5.5	520 ± 120	3.1 ± 2.6	120	78 ± 18	28 ± 13	13
T_9-Boc-T_5-Tas	5.9	450 ± 170	7.8 ± 3.0	41	58 ± 24	**33 ± 2.5**	20
T_3-Boc	**3.6**	520 ± 400	5.7 ± 3.5	87	60 ± 7.9	13 ± 6.6	11
T_6-Boc	4.7	430 ± 130	**9.3 ± 2.3**	**22**	89 ± 34	28 ± 15	13
T_9-Boc	4.8	440 ± 44	9.2 ± 5.1	**32**	56 ± 1.8	16 ± 5.8	**7.7**
T_3-Tas	**3.9**	550 ± 93	**9.5 ± 1.3**	44	66 ± 30	30 ± 7.4	11
T_6-Tas	4.7	500 ± 280	8.6 ± 2.6	**26**	67 ± 8.0	21 ± 5.7	15
T_9-Tas	4.6	480 ± 130	6.1 ± 4.3	43	66 ± 22	18 ± 11	16

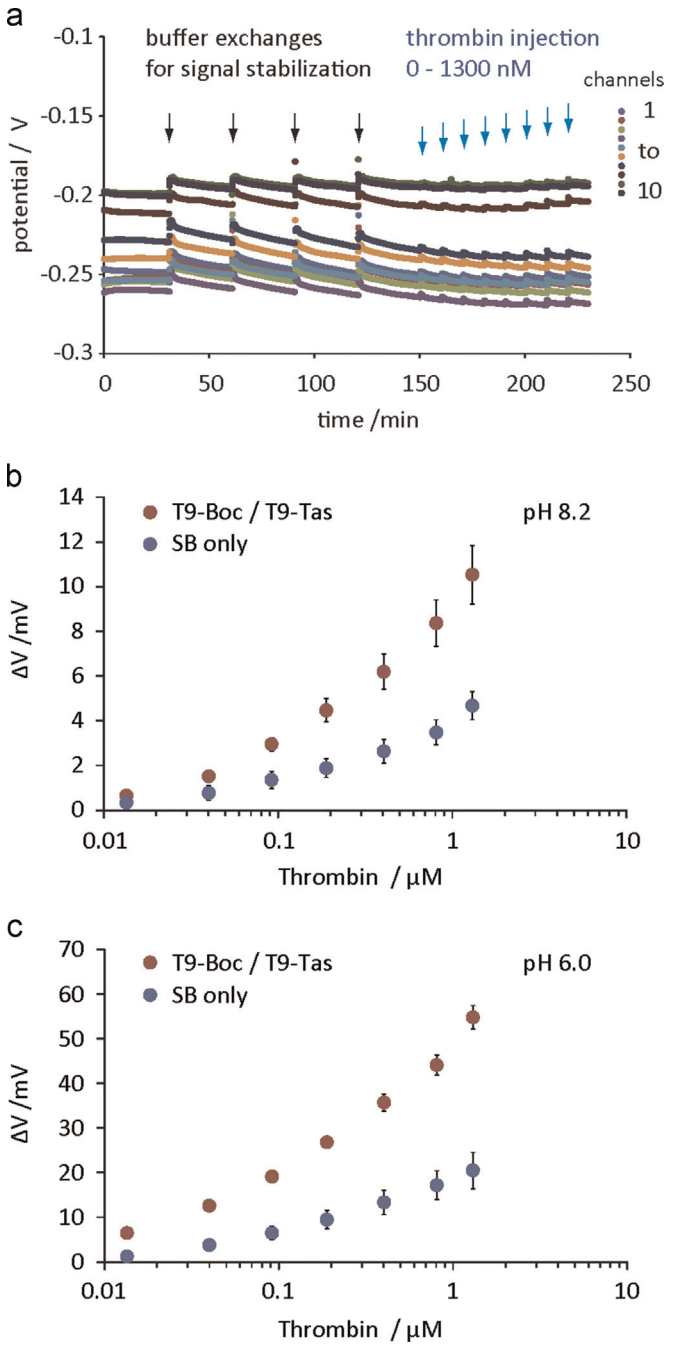

Fig. 3. Representative data on potentiometric biosensing of thrombin using the T_9-Boc/T_9-Tas aptamer-modified surface. (a) Real-time changes in the potential versus the Ag/AgCl reference electrode during the periods of signal stabilization (0–150 min) and thrombin titration (150–230 min) at pH 8.2 using a 10-channel gold microelectrode array. (b–c) Potential shifts as a function of bulk thrombin concentration on the aptamer-modified SB SAM and SB-only SAM surfaces at pH 8.2 (b) and pH 6.0 (c), respectively. Data were obtained by baseline calibration of the time-course of potential. $n=10$, average $\pm$ SD. RSD of the potentiometric signals was 11.8% and 5.0% at pH 8.2 and 6.0, respectively.

Miyahara, 2010, 2012b). Positive potential changes are attributed to positive charge density changes as a result of the binding of positively charged domain in thrombin onto the surface-immobilized aptamer within the electrical double layer as described in Eq. (1). In fact, the structural analysis of the thrombin–aptamer complex (PDB: 1HAO) using the eF-site software indicates a preferential arrangement of the positive domains as the epitope for anionic DNA aptamer (Kinoshita and Nakamura, 2005). The potential changes were more pronounced at pH 6.0 as compared with pH 8.2, due to the protonation of thrombin in the acidic environment (Fig. 3). A simple estimation of net-charges as a molecule from the sequences of light and heavy chains of thrombin using the protein calculator (Sillero and Maldonado, 2006) resulted in a dramatic increase in the overall valence number of +7.7 at pH 6.0 as compared with that of −0.2 at pH 8.2. The potential changes were small in control measurements of the binding assay on the electrode modified with the SB-only SAM (without aptamers) because of the lack of specific binding of thrombin onto the SB SAM. The sensitivity was +5.2 mV/log [*thrombin*] and +24.4 mV/log[*thrombin*] in the linear response regime in the semilogarithmic plots for the T_9-Boc/T_9-Tas surface at pH 8.2 and pH 6.0, respectively. The stability and reproducibility of potential from the 10-channel microelectrode were determined as RSD = 11.8% and 5.0% for T_9-Boc/T_9-Tas surface at pH 8.2 and 6.0, respectively.

To estimate the apparent binding affinity of thrombin on the dual aptamer surfaces, we analyzed the potentiometric data using the 1:1 Langmuir adsorption model. Since the surface charge density change (ΔQ) is proportional to the amount of captured biomolecule (Δm) as derived from Eq. (1); (Goda et al., 2012; Goda and Miyahara, 2010, 2012b).

$$\Delta V_{diff} = \Delta Q / C_{int} = q\Delta m / C \tag{5}$$

where ΔV_{diff} is the differential potentials obtained from the conditions with and without aptamers and q is the induced effective charge from single protein captured within the electrical double layer, respectively. Therefore, ΔV_{diff} can be described as a function of bulk thrombin concentration ([C]) from the Langmuir adsorption model using the apparent binding constant K_d as;

$$\Delta V_{diff} = [C]\Delta V_{max}/([C] + K_d) \tag{6}$$

or

$$\Delta V_{diff}{}^{-1} = (K_d/\Delta V_{max})[C]^{-1} + 1/\Delta V_{max} \tag{7}$$

Fig. 4 displays the results of curve fitting by least squares method from either Eqs. (6) or (7) to determine K_d and V_{max}. The apparent K_d was lower in the fitting using Eq. (7) by up to 10-fold as compared with Eq. (6) by primarily reflecting $\Delta V_{diff}{}^{-1}$ values at low [C] in the case of Eq. (7) (Table S2). However, the reproduced Langmuir isotherm from the binding parameters did not fit well with the experimental data at high [C]. Therefore, we used the parameters from direct curve fitting of the data using Eq. (6).

The fitting parameters for each condition are summarized in Table 1. For the dual aptamer surfaces at pH 8.2, K_d hit the lowest values for "T_9-Boc/T_6-Tas", "T_9-Boc/T_9-Tas", and "T_3-Boc-T_5-Tas". These K_d values were lower than those on the single aptamer surfaces. ΔV_{max} was slightly decreased in most of the dual aptamer surfaces compared with the single aptamer surfaces. The improved K_d and decreased ΔV_{max} suggest the occurrence of bivalent binding of thrombin by occupying the two aptamers on the two-component aptamer-modified surfaces. Among the dual aptamer surfaces, the longer thymine length for spacer and linker up to T_9 yielded higher ΔV_{max}. The binding parameters showed great improvements at pH 6.0, indicating a dominant effect of Coulombic forces for the affinity of aptamer–thrombin complex. K_d decreased by increasing the spacer lengths among the two-component aptamer surfaces. K_d was the best on the "T_3-Boc/T_9-Tas", "T_6-Boc/T_6-Tas" and "T_3-Boc-T_{10}-Tas" surfaces. ΔV_{max} was the highest on the dual aptamer surfaces ("T_3-Boc/T_3-Tas", "T_3-Boc-T_0-Tas" and "T_9-Boc-T_5-Tas"). The LOD reached 5.5 nM at pH 6.0. Performance of the dual aptamer-based potentiometric biosensor in terms of LOD was comparable to existing aptamer-based label-free techniques including surface plasmon resonance (Jalit et al., 2013; Kim et al., 2008a; Shevchenko et al., 2011), organic FET biosensor (Hammock

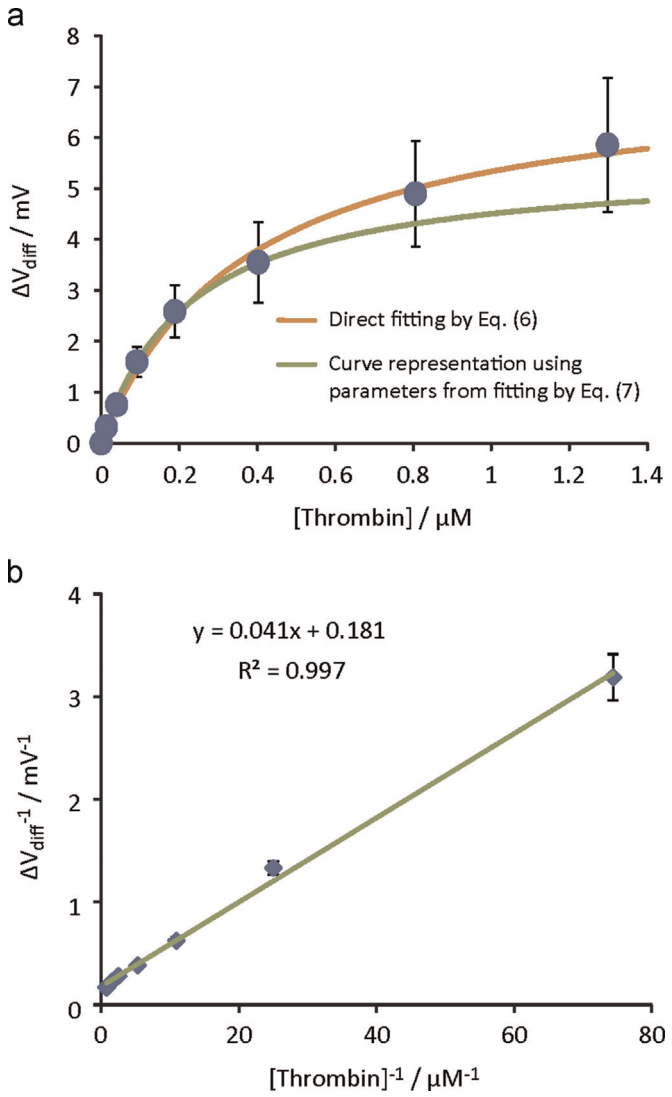

Fig. 4. Representative data on the curve fittings of thrombin signal from potentiometry on the T_9-Boc/T_9-Tas aptamer-modified surface at pH 8.2 for determining the binding parameters: K_d and ΔV_{max}. (a) Comparison of direct curve fitting of the signals by Eq. (6) with the represented curve from the fitting parameters obtained by the method as shown in (b) using Eq. (6). Plots were shown in average ± SD from single trial dataset ($n=10$). RSD of K_d and ΔV_{max} from three independent trials was 19% and 13%, respectively. (b) The result of linear fitting of the signal using Eq. (7). RSD of K_d and ΔV_{max} from three independent trials was 34% and 21%, respectively.

et al., 2013), and fluorescent aptasensor (Kong et al., 2013). Although some amplification-based or reagent-contained techniques show better detection limits down to picomolar levels (Cai et al., 2006; Guo et al., 2013; Hu et al., 2015; Jiang et al., 2013; Liu et al., 2014; Wang et al., 2013; Zhang et al., 2011), our technique may find an application with features on simplicity and high-throughput modality.

Previously, an order of magnitude enhancement in the affinity between thrombin and its aptamers by forming a serial connection of Bock and Tasset aptamers with T_5 linker in a solution phase was reported (Hasegawa et al., 2008). The slight improvements of the affinity via multiple bindings on the solid surface as compared with in solution phase suggest factors that impose restrictions for aptamer–protein binding at the solid–liquid interface (Cheng et al., 2007). First, molecular recognition on the surface is hindered by the inability to fold into a proper secondary structure, rendering some of the aptamers on the surface unavailable as a ligand. Second, binding of thrombin increases the charge at the interface, which in turn generates electrostatic repulsion to interfere with the binding of another target to adjacent aptamers. This may be the case because we used a decreased ionic strength to gain an electrical double layer thickness. Third, a surface-immobilized aptamer via relatively short spacer length impairs the freedom of Brownian motion, thus fails to reach to an epitope in a target molecule. Above results also indicate that the freedom of aptamer mobility is necessary to exert the original aptamer affinity by increasing the spacer length from the electrode surfaces. On the other hand, an increase in the distance of aptamer from the electrode surface is disadvantageous for the direct readout of innate biomolecular charges of captured protein within the electrical double layer ($\kappa^{-1} \sim 2.1$ nm) by decreasing the induced effective charge (q) shown in Eq. (5). Namely, to increase the mobility of graft aptamer chain and to improve the charge sensitivity for target protein is a trade-off relationship. Our study shows the importance in designing bio-interface at the molecular resolution. The best spacer length lies in between T_6 and T_9 for dual aptamer-based thrombin biosensing in potentiometry.

4. Conclusions

We developed an affordable method for improving the affinity of aptamer-modified sensor surface for thrombin in potentiometry by employing cooperative contacts using two different aptamer sequences that can target different epitopes in the protein molecule. The overall binding ability on the dual aptamer-modified surface exceeds the original binding capability of these aptamers used in an independent manner without synergy. The concept adds values to aptamer as a synthetic ligand by enhancing the sensitivity of aptamer-based biosensing to cope with immunosensing. The key technology lies in the design of spacer and liner in the probe molecules as a building component of SAM for making biorecognition interface within an electrical double layer.

Acknowledgments

This research was financed by the Grant-in-Aid for Scientific Research on Innovative Areas “Nanomedicine Molecular Science” (#26107705) from MEXT of Japan, Grant-in-Aid for Scientific Research C (#15K05530) from JSPS, Futaba Electronics Foundation, and the Center of Innovation (COI) Program from Japan Science and Technology Agency (JST).

Appendix A. Supplementary material

Supplementary data associated with this article can be found in the online version at http://dx.doi.org/10.1016/j.bios.2015.05.067

References

Bergveld, P., 2003. Sensor Actuat. B: Chem. 88 (1), 1–20.
Bock, L.C., Griffin, L.C., Latham, J.A., Vermaas, E.H., Toole, J.J., 1992. Nature 355 (6360), 564–566.
Bode, W., Mayr, I., Baumann, U., Huber, R., Stone, S.R., Hofsteenge, J., 1989. EMBO J. 8 (11), 3467–3475.
Borissoff, J.I., Spronk, H.M., Heeneman, S., ten Cate, H., 2009. Cardiovasc. Res. 82 (3), 392–403.
Bukar, N., Zhao, S.S., Charbonneau, D.M., Pelletier, J.N., Masson, J.F., 2014. Chem. Commun. 50 (38), 4947–4950.
Cai, H., Lee, T.M.H., Hsing, I.M., 2006. Sensor Actuat. B: Chem. 114 (1), 433–437.
Cheng, A.K.H., Ge, B., Yu, H.Z., 2007. Anal. Chem. 79 (14), 5158–5164.
Darmostuk, M., Rimpelova, S., Gbelcova, H., Ruml, T., 2015. Biotechnol. Adv. . http://dx.doi.org/10.1016/j.biotechadv.2015.1002.1008, in press

Elfstrom, N., Karlstrom, A.E., Linnros, J., 2008. Nano Lett. 8 (3), 945–949.
Elnathan, R., Kwiat, M., Pevzner, A., Engel, Y., Burstein, L., Khatchtourints, A., Lichtenstein, A., Kantaev, R., Patolsky, F., 2012. Nano Lett. 12 (10), 5245–5254.
Famulok, M., Mayer, G., 2011. Acc. Chem. Res. 44 (12), 1349–1358.
Goda, T., Maeda, Y., Miyahara, Y., 2012. Anal. Chem. 84 (17), 7308–7314.
Goda, T., Miyahara, Y., 2010. Anal. Chem. 82 (5), 1803–1810.
Goda, T., Miyahara, Y., 2012a. Biosens. Bioelectron. 32 (1), 244–249.
Goda, T., Miyahara, Y., 2012b. Langmuir 28 (41), 14730–14738.
Goda, T., Miyahara, Y., 2013. Biosens. Bioelectron. 45, 89–94.
Goda, T., Tabata, M., Miyahara, Y., 2015. Front. Bioeng. Biotechnol. 3, 29.
Graham, A.H.D., Robbins, J., Bowen, C.R., Taylor, J., 2011. Sensors 11 (5), 4943–4971.
Guo, Y.J., Han, Y.J., Guo, Y.X., Dong, C., 2013. Biosens. Bioelectron. 45, 95–101.
Hammock, M.L., Knopfmacher, O., Naab, B.D., Tok, J.B.H., Bao, Z.A., 2013. ACS Nano 7 (5), 3970–3980.
Hasegawa, H., Taira, K.I., Sode, K., Ikebukuro, K., 2008. Sensors 8 (2), 1090–1098.
Holmlin, R.E., Chen, X.X., Chapman, R.G., Takayama, S., Whitesides, G.M., 2001. Langmuir 17 (9), 2841–2850.
Hu, Y.F., Shen, Q.P., Li, W., Liu, Z.L., Nie, Z., Yao, S.Z., 2015. Biosens. Bioelectron. 63, 331–338.
Im, H.S., Huang, X.J., Gu, B., Choi, Y.K., 2007. Nat. Nanotechnol. 2 (7), 430–434.
Jalit, Y., Gutierrez, F.A., Dubacheva, G., Goyer, C., Coche-Guerente, L., Defrancq, E., Labbe, P., Rivas, G.A., Rodriguez, M.C., 2013. Biosens. Bioelectron. 41, 424–429.
Jayasena, S.D., 1999. Clin. Chem. 45 (9), 1628–1650.
Jiang, C.F., Zhao, T.T., Li, S., Gao, N.Y., Xu, Q.H., 2013. ACS Appl. Mater. Interface 5 (21), 10853–10857.
Jie, G., Yuan, J., 2012. Anal. Chem. 84 (6), 2811–2817.
Kim, A., Ah, C.S., Park, C.W., Yang, J.H., Kim, T., Ahn, C.G., Park, S.H., Sung, G.Y., 2010. Biosens. Bioelectron. 25 (7), 1767–1773.
Kim, D.K., Kerman, K., Hiep, H.M., Saito, M., Yamamura, S., Takamura, Y., Kwon, Y.S., Tamiya, E., 2008a. Anal. Biochem. 379 (1), 1–7.
Kim, J.P., Lee, B.Y., Hong, S., Sim, S.J., 2008b. Anal. Biochem. 381 (2), 193–198.
Kinoshita, K., Nakamura, H., 2005. Protein Sci. 14 (3), 711–718.
Kong, L., Xu, J., Xu, Y.Y., Xiang, Y., Yuan, R., Chai, Y.Q., 2013. Biosens. Bioelectron. 42, 193–197.
Lee, C.S., Kim, S.K., Kim, M., 2009. Sensors 9 (9), 7111–7131.
Lee, J.O., So, H.M., Jeon, E.K., Chang, H., Won, K., Kim, Y.H., 2008. Anal. Bioanal. Chem. 390 (4), 1023–1032.
Li, D., Song, S., Fan, C., 2010. Acc. Chem. Res. 43 (5), 631–641.
Liang, G.H., Cai, S.Y., Zhang, P., Peng, Y.Y., Chen, H., Zhang, S., Kong, J.L., 2011. Anal. Chim. Acta 689 (2), 243–249.
Lin, T.W., Hsieh, P.J., Lin, C.L., Fang, Y.Y., Yang, J.X., Tsai, C.C., Chiang, P.L., Pan, C.Y., Chen, Y.T., 2010. Proc. Natl. Acad. Sci. USA 107 (3), 1047–1052.
Liu, S., Lin, Y., Wang, L., Liu, T., Cheng, C., Wei, W., Tang, B., 2014. Anal. Chem. 86 (8), 4008–4015.
Loo, A.H., Bonanni, A., Pumera, M., 2012. Nanoscale 4 (1), 143–147.
Mammen, M., Choi, S.K., Whitesides, G.M., 1998. Angew. Chem. Int. Ed. 37 (20), 2755–2794.
Matsumoto, A., Sato, N., Sakata, T., Yoshida, R., Kataoka, K., Miyahara, Y., 2009. Adv. Mater. 21 (43), 4372–4378.
Nierodzik, M.L., Karpatkin, S., 2006. Cancer Cell 10 (5), 355–362.
Palazzo, G., De Tullio, D., Magliulo, M., Mallardi, A., Intranuovo, F., Mulla, M.Y., Favia, P., Vikholm-Lundin, I., Torsi, L., 2015. Adv. Mater. 27 (5), 911–916.
Palchetti, I., Mascini, M., 2012. Anal. Bioanal. Chem. 402 (10), 3103–3114.
Poghossian, A., Cherstvy, A., Ingebrandt, S., Offenhausser, A., Schoning, M.J., 2005. Sensor Actuat. B: Chem. 111, 470–480.
Poirier, G.E., Tarlov, M.J., 1994. Langmuir 10 (9), 2853–2856.
Schoning, M.J., Poghossian, A., 2006. Electroanalysis 18 (19-20), 1893–1900.
Shevchenko, Y., Francis, T.J., Blair, D.A.D., Walsh, R., DeRosa, M.C., Albert, J., 2011. Anal. Chem. 83 (18), 7027–7034.
Sillero, A., Maldonado, A., 2006. Comput. Biol. Med. 36 (2), 157–166.
Smith, R.S., Zhang, Z., Bouchard, M., Li, J., Lapp, H.S., Brotske, G.R., Lucchino, D.L., Weaver, D., Roth, L.A., Coury, A., Biggerstaff, J., Sukavaneshvar, S., Langer, R., Loose, C., 2012. Sci. Transl. Med. 4 (153), 153ra132.
Smith, S.B., Cui, Y.J., Bustamante, C., 1996. Science 271 (5250), 795–799.
Steel, A.B., Herne, T.M., Tarlov, M.J., 1998. Anal. Chem. 70 (22), 4670–4677.
Stern, E., Klemic, J.F., Routenberg, D.A., Wyrembak, P.N., Turner-Evans, D.B., Hamilton, A.D., LaVan, D.A., Fahmy, T.M., Reed, M.A., 2007a. Nature 445 (7127), 519–522.
Stern, E., Vacic, A., Rajan, N.K., Criscione, J.M., Park, J., Ilic, B.R., Mooney, D.J., Reed, M. A., Fahmy, T.M., 2010. Nat. Nanotechnol. 5 (2), 138–142.
Stern, E., Wagner, R., Sigworth, F.J., Breaker, R., Fahmy, T.M., Reed, M.A., 2007b. Nano Lett. 7 (11), 3405–3409.
Stoltenburg, R., Reinemann, C., Strehlitz, B., 2007. Biomol. Eng. 24 (4), 381–403.
Tang, X.H., Jonas, A.M., Nysten, B., Demoustier-Champagne, S., Blondeau, F., Prevot, P.P., Pampin, R., Godfroid, E., Iniguez, B., Colinge, J.P., Raskin, J.P., Flandre, D., Bayot, V., 2009. Biosens. Bioelectron. 24 (12), 3531–3537.
Tasset, D.M., Kubik, M.F., Steiner, W., 1997. J. Mol. Biol. 272 (5), 688–698.
Taylor, A.I., Arangundy-Franklin, S., Holliger, P., 2014. Curr. Opin. Chem. Biol. 22, 79–84.
Wang, X., Dong, P., Yun, W., Xu, Y., He, P., Fang, Y., 2009. Biosens. Bioelectron. 24 (11), 3288–3292.
Wang, X.Y., Gao, A., Lu, C.C., He, X.W., Yin, X.B., 2013. Biosens. Bioelectron. 48, 120–125.
Yang, D.F., Wilde, C.P., Morin, M., 1996. Langmuir 12 (26), 6570–6577.
Zhang, H.Y., Stockley, P.G., Zhou, D.J., 2011. Faraday Discuss. 149, 319–332.
Zheng, G.F., Patolsky, F., Cui, Y., Wang, W.U., Lieber, C.M., 2005. Nat. Biotechnol. 23 (10), 1294–1301.
Zhou, J., Battig, M.R., Wang, Y., 2010. Anal. Bioanal. Chem. 398 (6), 2471–2480.